Acta Crystallographica Section B
Structural Science
ISSN 0108-7681

Structures and phase transitions of the A_7PSe_6 (A = Ag, Cu) argyrodite-type ionic conductors. II. β- and γ-Cu_7PSe_6

E. Gaudin,[a] F. Boucher,[a] V. Petricek,[b] F. Taulelle[c] and M. Evain[a]*

[a]Laboratoire de Chimie des Solides, IMN, UMR C6502 CNRS, Université de Nantes, 2 rue de la Houssinière, BP 32229, 44322 Nantes CEDEX 3, France, [b]Institute of Physics, Academy of Sciences of the Czech Republic, Na Slovance 2, 180 40 Praha 8, Czech Republic, and [c]RMN et Chimie du Solide, UMR 7510 CNRS, Universite Louis Pasteur, Institut Le Bel, 4 rue Blaise Pascal, 67070 Strasbourg CEDEX, France

Correspondence e-mail: evain@cnrs-imn.fr

Received 20 September 1999
Accepted 20 December 1999

The crystal structures of two of the three polymorphic forms of the Cu_7PSe_6 argyrodite compound are determined by means of single-crystal X-ray diffraction. In the high-temperature form, at 353 K, *i.e.* 33 K above the first phase transition, γ-Cu_7PSe_6 crystallizes in cubic symmetry, space group $F\bar{4}3m$. The full-matrix least-squares refinement of the structure leads to the residual factors $R = 0.0201$ and $wR = 0.0245$ for 31 parameters and 300 observed independent reflections. In the intermediate form, at room temperature, β-Cu_7PSe_6 crystallizes again in cubic symmetry, but with space group $P2_13$. Taking into account a merohedric twinning, the refinement of the β-Cu_7PSe_6 structure leads to the residual factors $R = 0.0297$ and $wR = 0.0317$ for 70 parameters and 874 observed, independent reflections. The combination of a Gram–Charlier development of the Debye–Waller factor and a split model for copper cations reveals the possible diffusion paths of the d^{10} species in the γ-Cu_7PSe_6 ionic conducting phase. The partial ordering of the Cu^+ d^{10}element at the phase transition is found in concordance with the highest probability density sites of the high-temperature phase diffusion paths. A comparison between the two Cu_7PSe_6 and Ag_7PSe_6 analogues is carried out, stressing the different mobility of Cu^+ and Ag^+ and their relative stability in low-coordination chalcogenide environments.

1. Introduction

In part I of our study on the A_7PSe_6 (A = Ag, Cu) argyrodite-type ionic conductors (Evain *et al.*, 1998), we reported on the structure determination of the β-Ag_7PSe_6 and γ-Ag_7PSe_6 polymorphic forms and we explained the $\gamma \rightarrow \beta$ phase transition in terms of cation ordering. In particular, we explained the diffusion paths which the Ag^+ d^{10} cations follow through the $[PSe_6]$ structural skeleton of the γ-Ag_7PSe_6 high-temperature polymorphic form and showed that those cations localized, at the transition toward the β low-temperature form, in the most pronounced probability density areas of the diffusion paths. Those preferential sites could be either linear, triangular or tetrahedral, in agreement with the low coordination sites usually observed for Ag^+.

After the analysis of the Ag_7PSe_6 phases, we focused our attention on a closely related system, Cu_7PSe_6. Although similar to Ag_7PSe_6 in many respects, Cu_7PSe_6 contrasts by presenting two structural transitions. The interest for a comprehensive study of the three Cu_7PSe_6 polymorphic forms is twofold. On one hand the study should reveal the origin of the second transition, on the other hand it should indicate the structural modifications implied by the d^{10} cation change; Cu^+ being expected to be less prone to low chalcogenide coordi-

nation than Ag^+. In the present paper, part II of our study on the A_7PSe_6 system, we report on the structure determination of γ-Cu_7PSe_6 and β-Cu_7PSe_6 and compare the two phases to their silver analogues. The low-temperature α-Cu_7PSe_6 phase will be analyzed in a separate paper, part III, since the determination of its structure is not straightforward owing to a severe multiple twinning and requires extensive MAS NMR (magic angle spinning solid-state NMR) analyses.

2. Experimental

2.1. Synthesis and characterization

A sealed evacuated quartz tube loaded with Cu, P and Se elements in stoichiometric proportions (Cu:P:Se = 7:1:6; Cu: wire 99.9%, Fluka; Se: pearls 99.995%, Fluka; P: puriss powder, Fluka) was heated for a week at 1093 K, *i.e.* slightly above the Cu_7PSe_6 melting temperature of *ca* 1068 K (Kuhs *et al.*, 1977; Andrae & Blachnik, 1993). Good quality, metallic-like crystals are then obtained after grinding the as-prepared product and heating it again at 973 K for 2 weeks. EDXS (energy dispersive X-ray spectroscopy) analysis of several crystals by means of a Jeol microscope (PGT-IMIX-PTS equipped Jeol-JSM5800LV) confirmed the phase composition. Complementary room-temperature powder X-ray diffractograms did not indicate the presence of potential impurities. A DSC (differential scanning calorimetry) analysis (from 173 to 523 K at 5 K min^{-1} on a DSC121 Setaram apparatus) unambiguously revealed two endothermic peaks at 250 (1) and 320 (1) K corresponding to the $\alpha \rightarrow \beta$ and $\beta \rightarrow \gamma$ phase transitions, respectively.

2.2. Data collection

In order to minimize bias from crystal shape on the absorption corrections, Cu_7PSe_6 spheres were formed from large single crystals by means of an air-blowing abrasive device. A first sphere, 0.069 mm in radius, was glued at the tip of a quartz capillary by means of a Torr Seal vacuum sealing kit. An AET hot nitrogen gas-blowing equipment was used for the high-temperature data collection (353 K, *i.e.* 33 K above the phase transition) on a Nonius CAD-4*F* diffractometer (graphite-monochromated Mo K-$L_{2,3}$ radiation, λ = 0.71073 Å), with the temperature controlled to within ± 1 K. The collection was carried out in an azimuthal mode ($\psi = 20^\circ$) to minimize thermal expansion effects of the support. A larger sphere, 0.086 mm in radius, was used for the room-temperature and subsequent measurements (see below). To further reduce the absorption effect and therefore ease the symmetry analysis, the room-temperature data collection was carried out on a Siemens P4 diffractometer using graphite-monochromated Ag radiation (λ = 0.5609 Å). For both data collections (high- and room-temperature), the observed intensity decay was less than 1%.

2.3. Data processing

After the Lorentz–polarization treatment, the intensities were analytically corrected for absorption using a spherical model. All calculations were carried out with the *JANA*98 program package (Petricek & Dusek, 1998). For the high-temperature data set, the averaging suggested the same point group as for γ-Ag_7PSe_6, *i.e.* $\bar{4}3m$ [$R_{int}(I)$ = 0.034]. The symmetry determination of the room-temperature set was, however, less straightforward since averaging with the 23 and $\bar{4}3m$ point-group symmetries led to $R_{int}(I)$ = 0.057 and 0.092, respectively. The rather small difference in $R_{int}(I)$ values for the two point-group symmetries suggested a possible twinning. Data collections carried out for two new single crystals (hereafter referred to as crystal RT2 and RT3) confirmed this possibility with 23 as the most probable point group for RT2 and 23 and $\bar{4}3m$ being equivalent for RT3. Based upon previous powder studies (Kuhs *et al.*, 1977), which suggested $P2_13$ as the possible space group, and considering the fact that the β-Ag_7PSe_6 structure was solved with $P2_13$ as a space group, 23 was chosen as the real point-group symmetry. For both refinements, scattering factors and anomalous dispersion correction terms were taken from Maslen *et al.* (1992) and Creagh & McAuley (1992), respectively. The ionic conductor character of the high-temperature polymorphic form required a refinement procedure mixing a split-model distribution and a Gram–Charlier non-harmonic[1] development of the Debye–Waller factor (Johnson & Levy, 1974; Kuhs, 1984) for the Cu^+ ions. This approach was also used for the description of one copper of the room-temperature form. In the two refinement sets, the overall copper stoichiometry was constrained to that imposed by the Cu_7PSe_6 formula, in agreement with both the charge balance and the chemical analysis. The refinements were performed on F by minimizing the $wR = [\sum w(|F_o| - |F_c|)^2/\sum w|F_o|^2]^{1/2}$ function, with a weighting factor, w, based on $\sigma(F_o)$ and using all reflections (see Table 1).[2]

3. Results

3.1. γ-Cu_7PSe_6 (353 K)

Since no systematic absences could be found in addition to those related to the F centering, $F\bar{4}3m$ was chosen as the probable space group ($F\bar{4}3m$ is a space group common to most argyrodite high-temperature polymorphic forms). The structure refinement was initiated with the positions observed in Ag_7PSe_6. With isotropic displacement parameters (IDPs), the residual factor smoothly converged to R = 0.075 (wR = 0.096). The introduction of anisotropic displacement parameters (ADPs) reduced that value to R = 0.046 (wR = 0.053). However, a damping factor had to be applied to stabilize the refinement procedure. The subsequent application of an isotropic secondary extinction (Becker & Coppens, 1974) considerably lowered the residual value to R = 0.028 (wR = 0.024). Difference-Fourier map analyses then revealed significant residues around Cu1 (similar to those observed at that

[1] Clearly, in the case of ion conductivity, the deformation is due to atomic disorder and not intrinsic anharmonicity, thus the general term 'non-harmonic' is used throughout the paper.

[2] Supplementary data for this paper are available from the IUCr electronic archives (Reference: LC0017). Services for accessing these data are described at the back of the journal.

Table 1
Experimental details.

	β-Cu_7PSe_6	γ-Cu_7PSe_6
Crystal data		
Chemical formula weight	949.56	949.56
Cell setting	Cubic	Cubic
Space group	$P2_13$	$F\bar{4}3m$
a (Å)	10.1080 (4)	10.1130 (10)
b (Å)	10.1080 (4)	10.1130 (10)
c (Å)	10.1080 (4)	10.1130 (10)
V (Å^3)	1032.75 (12)	1034.3 (3)
Z	4	4
D_x (Mg m^{-3})	6.105	6.096
Radiation type	Ag $K\alpha$	Mo $K\alpha$
Wavelength (Å)	0.56090	0.71073
No. of reflections for cell parameters	34	25
μ (mm^{-1})	18.628	35.32
F(000)	1688	1688
Temperature (K)	293	353
Crystal form	Sphere	Sphere
Crystal radius (mm)	0.086	0.069
Crystal colour	Metallic lustre	Metallic lustre
Data collection		
Diffractometer	Siemens $P4$	Enraf–Nonius CAD-4
Monochromator	Oriented graphite (002)	Oriented graphite (002)
Data collection method	θ scans	ω–θ scans
Absorption correction	Spherical	Spherical
T_{min}	0.1123	0.0452
T_{max}	0.1358	0.0878
No. of measured reflections	10 070	1726
No. of independent reflections	1627	368
No. of observed reflections	874	300
Criterion for observed reflections	$I > 3.0\sigma(I)$	$I > 3.0\sigma(I)$
R_{int}	0.057	0.034
$\sin\theta/\lambda$ (Å^{-1})	0.823	0.904
No. of standard reflections	3	3
Frequency of standard reflections	Every 60 min	Every 100 reflections
Refinement		
Refinement on	F	F
R	0.0297	0.0201
wR	0.0317	0.0245
S	0.80	1.09
No. of reflections used in refinement	874	300
No. of parameters used	70	31
$(\delta/\sigma)_{max}$	< 0.0001	< 0.0001
Weighting scheme	$w = 1/[\sigma^2\lvert F_o\rvert + (0.016\lvert F_o\rvert)^2]$	$w = 1/[\sigma^2\lvert F_o\rvert + (0.015\lvert F_o\rvert)^2]$
$\Delta\rho_{max}$ (e Å^{-3})	1.89	0.69
$\Delta\rho_{min}$ (e Å^{-3})	−1.14	−0.76
Extinction method	Type I, Gaussian (Becker & Coppens, 1974)	Type I, Gaussian (Becker & Coppens, 1974)
Extinction coefficient	0.1056 (4)	0.172 (8)

stage of the refinement around Ag1 in γ-Ag_7PSe_6). A meaningful development of the Cu1 Debye–Waller factor up to the third order by means of a Gram–Charlier expansion reduced the difference-Fourier residues to a non-significant noise. The final residual factor took the value $R = 0.0201$ ($wR = 0.0245$) for 31 parameters and 300 observed independent reflections (see Table 1 for details). The final refined atomic parameters for γ-Cu_7PSe_6 are given in Tables 2, 3 and 4.

3.2. β-Cu_7PSe_6 (293 K)

In a first step, the refinement was carried out with the RT1 crystal and the $P2_13$ space group, expected from the previous powder studies and used in the β-Ag_7PSe_6 structure refinement. The positions of β-Ag_7PSe_6 were taken as a starting point. With IDPs the refinement led to $R = 0.153$ ($wR = 0.190$). Introducing ADPs lowered that value to $R = 0.095$ ($wR = 0.119$). Taking into account the third-order tensor for the copper Debye–Waller factor only reduces the residual factor to $R = 0.077$ ($wR = 0.101$). At that stage, analyses of the difference-Fourier maps did not show any characteristic features, but to a uniform noise level.

New data collections were then performed on two different crystals (RT2 and RT3, see above). Similar refinement procedures for these sets gave $R = 0.055$ (RT2 set) and $R = 0.122$ (RT3 set). It was then clear that the model found for the RT1 data set could not be generalized to the other sets. A possible twinning was therefore looked for. By correlating the apparent symmetry and the residual factors (23 as the most probable point group for the lowest R value and both 23 and $\bar{4}3m$ as a possible point group for the highest R value) the $\bar{4}$ symmetry operation was chosen as the twin law, with regard to the cosets formed with respect to the 23 subgroup. Introducing that law for RT1 dramatically improved the results with an R value setting at 0.045 ($wR = 0.049$) for a twin fraction of 24.1%. Similar results were obtained for RT2 and RT3 with twin fractions of 3.3 and 55.1%, respectively. The RT1 set giving the best final results will be from now on the only one fully described in the analysis.

New difference-Fourier map analyses revealed important residues around Cu2, the third-order Gram–Charlier non-harmonic terms being inadequate for a proper density description. Going back to a refinement with a second-order tensor for Cu2 (*i.e.* ADPs), the difference-Fourier maps suggested a splitting of Cu2. It is worth noticing that non-harmonic developments of the Debye–Waller factor are particularly efficient for small splitting (they considerably reduce the correlation effects for approximately the same

Table 2
Fractional atomic coordinates and equivalent isotropic displacement parameters (Å^2).

$$U_{eq} = (1/3)\Sigma_i\Sigma_j U^{ij} a^i a^j \mathbf{a}_i.\mathbf{a}_j.$$

	x	*y*	*z*	U_{eq}	Site occupancy
β-Cu_7PSe_6 ($P2_13$, T = 293 K)					
P	0.7485 (2)	0.7485	0.7485	0.0103 (2)	
Se1*a*	0.87477 (9)	0.87477	0.87477	0.0148 (2)	
Se1*b*	0.37079 (11)	0.37645 (11)	0.88083 (10)	0.0134 (3)	
Se2	0.23601 (11)	0.23601	0.23601	0.0210 (2)	
Se3	0.49079 (12)	0.49079	0.49079	0.0221 (2)	
Cu1	0.0720 (3)	−0.0892 (3)	−0.2696 (3)	0.0463 (6)	
Cu2*a*	0.0024 (9)	0.0034 (9)	0.2795 (2)	0.059 (2)	0.68 (2)
Cu2*b*	0.0636 (11)	0.0578 (8)	0.2639 (8)	0.032 (2)	0.32
Cu3	0.3608 (5)	0.3608	0.3608	0.199 (3)	
γ-Cu_7PSe_6 ($F\bar{4}3m$, T = 353 K)					
P	3/4	3/4	3/4	0.0098 (2)	
Se1	0.87576 (5)	0.87576	0.87576	0.01623 (7)	
Se2	1/4	1/4	1/4	0.0330 (2)	
Se3	1/2	1/2	1/2	0.0273 (2)	
Cu1	0.0787 (8)	0.0787	0.2673 (6)	0.0511 (10)	0.314 (11)
Cu2	0.016 (3)	0.016	0.2757 (8)	0.068 (10)	0.179 (9)
Cu3	0.1286 (8)	0.1286	0.3714	0.243 (11)	0.27

Table 3
Anisotropic displacement parameters U^{ij} (Å^2).

The anisotropic displacement factor exponent takes the form: $-2\pi^2\Sigma_i\Sigma_j U^{ij} a_i^* a_j^* h_i h_j$.

	U^{11}	U^{22}	U^{33}	U^{12}	U^{13}	U^{23}
β-Cu_7PSe_6 ($P2_13$, T = 293 K)						
P	0.0103 (4)	0.0103	0.0103	−0.0002 (9)	−0.0002	−0.0002
Se1*a*	0.0148 (4)	0.0148	0.0148	−0.0026 (4)	−0.0026	−0.0026
Se1*b*	0.0132 (5)	0.0145 (5)	0.0124 (5)	−0.0029 (4)	−0.0018 (3)	−0.0026 (3)
Se2	0.0210 (4)	0.0210	0.0210	0.0022 (4)	0.0022	0.0022
Se3	0.0221 (4)	0.0221	0.0221	0.0041 (4)	0.0041	0.0041
Cu1	0.0316 (9)	0.0495 (11)	0.0579 (11)	−0.0029 (8)	0.0025 (8)	0.0003 (10)
Cu2*a*	0.077 (5)	0.080 (5)	0.0213 (9)	0.056 (4)	0.010 (2)	0.005 (2)
Cu2*b*	0.036 (4)	0.032 (3)	0.028 (3)	0.005 (3)	0.004 (3)	−0.003 (2)
Cu3	0.199 (5)	0.199	0.199	−0.088 (3)	−0.088	−0.088
γ-Cu_7PSe_6 ($F\bar{4}3m$, T = 353 K)						
P	0.0098 (3)	0.0098	0.0098	0	0	0
Se1	0.01622 (12)	0.01622	0.01622	−0.00362 (7)	−0.00362	−0.00362
Se2	0.0330 (4)	0.0330	0.0330	0	0	0
Se3	0.0273 (4)	0.0273	0.0273	0	0	0
Cu1	0.0479 (14)	0.0479	0.057 (2)	0.004 (2)	−0.0008	−0.0008
Cu2	0.09 (2)	0.09	0.030 (3)	0.06 (2)	−0.019 (9)	−0.019
Cu3	0.24 (2)	0.24	0.24	−0.101 (10)	−0.101	−0.101

number of parameters), but are not suitable for large splitting (they require many more parameters than a simple splitting which is then stable). Indeed, the splitting of Cu2 in Cu2*a* and Cu2*b* and the use of ADPs for those two atoms further reduced the residual values (R = 0.039 and wR = 0.042) for the same number of parameters (69). Finally, an examination of the $|F_o| - |F_c|$ for different *hkl* reflection classes revealed mainly positive differences for the reflections which verified the *F* centering condition and mainly negative differences for those which transgressed the condition, the latter reflections being much weaker in intensity. From that observation, the introduction of two different scale factors considerably improved the results, yielding the following final residual factors: R = 0.0297 and wR = 0.0317. The use of a second scale factor for the reflections violating the *F* centering condition is to be related to a partial integration of the intensities, because of a diffuse character of the reflections. It is worth noticing that those reflections are only satellites introduced by the ordering of the Cu atoms, their diffuse character being related to a lack of long-range order intrinsic to the phase and/or induced by the twinning. Such a procedure led to reproducible results for the RT1, RT2 and RT3 data sets. The final refined atomic site parameters for β-Cu_7PSe_6 are given in Tables 2, 3 and 4.

4. Discussion

The Cu_7PSe_6 argyrodite structure can be considered as a $[PSe_6]$ framework in which the Cu^+ d^{10} cations occupy various linear, triangular or tetrahedral sites. In turn, the $[PSe_6]$ framework can be described as a c.c.p. (cubic close-packed) array of Se^{2-} anions with extra Se^{2-} anions and $[PSe_4]^{3-}$ tetrahedral units alternatively occupying the tetrahedral holes (see Fig. 1).

4.1. γ-Cu_7PSe_6 (353 K)

The structure framework is very similar to that of γ-Ag_7PSe_6. For instance, the calculated P—Se distances of the $[PSe_4]$ tetrahedral units (2.20 Å) are close to those found in γ-Ag_7PSe_6 (2.22 Å), and in agreement with the distances expected from Shannon's tables (2.19 Å; Shannon, 1981). However, it is worth noticing that the equivalent IDPs of the γ-Cu_7PSe_6 framework atoms are smaller than their counterparts in γ-Ag_7PSe_6 at 353 K [*e.g.* U_{eq}(P) = 0.010 Å^2 to be compared with U_{eq}(P) = 0.021 Å^2, respectively].

As for previously described argyrodite high-temperature poymorphic forms (Boucher *et al.*, 1993; Evain *et al.*, 1998), the combination of a split-atom model and of a non-harmonic development of the Debye–Waller factor in the structure determination clearly showed the diffusion paths which the Cu^+ d^{10} ions follow in γ-Cu_7PSe_6. This distribution of Cu atoms is in agreement with the ionic character expected for an

Table 4
Non-harmonic displacement parameters.

β-Cu_7PSe_6 ($P2_13$, T = 293 K)

	C_{GC}^{111}	C_{GC}^{112}	C_{GC}^{113}	C_{GC}^{122}	C_{GC}^{123}
Cu1 (1)	−0.0004 (6)	0.0018 (4)	−0.0010 (5)	−0.0033 (5)	−0.0008 (4)

	C_{GC}^{133}	C_{GC}^{222}	C_{GC}^{223}	C_{GC}^{233}	C_{GC}^{333}
Cu1 (1)	0.0034 (5)	−0.0047 (9)	−0.0022 (6)	−0.0073 (6)	0.0030 (9)

	$C_{GC}^{111} = C_{GC}^{222} = C_{GC}^{333}$	$C_{GC}^{112} = C_{GC}^{133} = C_{GC}^{223}$	$C_{GC}^{113} = C_{GC}^{122} = C_{GC}^{233}$	C_{GC}^{123}
Cu3 (.3.)	−0.068 (6)	0.040 (5)	0.003 (5)	−0.034 (5)

γ-Cu_7PSe_6 ($F\bar{4}3m$, T = 353 K)

	$C_{GC}^{111} = C_{GC}^{222}$	$C_{GC}^{112} = C_{GC}^{122}$	$C_{GC}^{113} = C_{GC}^{223}$	C_{GC}^{123}	$C_{GC}^{133} = C_{GC}^{223}$	C_{GC}^{333}
Cu1 (..m)	0.0049 (8)	−0.0021 (5)	0.0018 (5)	−0.0018 (5)	0.0062 (6)	−0.0052 (12)

Third-order tensor elements C_{GC}^{pqr} [Kuhs, 1983, eq. (3)] are multiplied by 10^3.

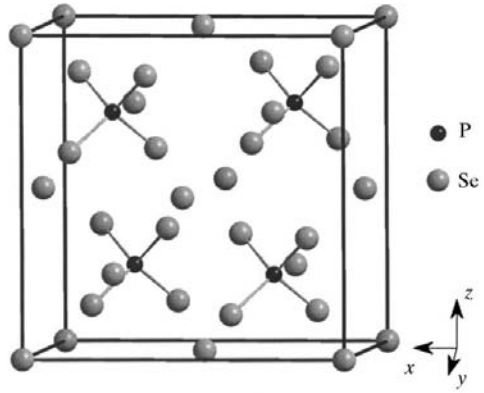

Figure 1
The cubic [PSe_6] framework of γ-Cu_7PSe_6.

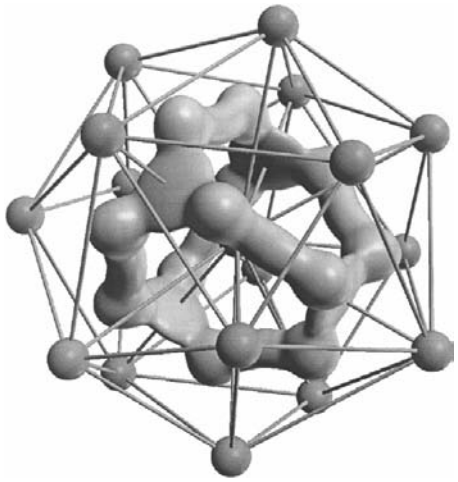

Figure 2
Three-dimensional representation of the joint probability density isosurface (at the 90 Å^{-3} level) for γ-Cu_7PSe_6 at 353 K, showing copper diffusion paths within a cluster centered on Se3. Se atoms are represented as spheres of arbitrary size.

argyrodite high-temperature polymorphic form and is confirmed by concomitant ^{63}Cu NMR measurements which show that the various copper sites cannot be identified, only one exchange peak being observed. As depicted in Fig. 2, the copper electron density is maximum around Se3, giving rise to an apparent cluster. Clearly, this electron density is much more dense than in γ-Ag_7PSe_6. This is confirmed by a lack of connection between the clusters throughout the structure as shown in Fig. 3 (a similar joint probability density isosurface at the same level gave rise to a connection of the clusters in γ-Ag_7PSe_6). This is also confirmed by much higher density probabilities at the mode positions (*i.e.* positions at the density maximums; see the section presented in Fig. 4), with 2211, 2010 and 271 Å^{-3} for Cu1*, Cu2* and Cu3* *versus* 880 and 188 Å^{-3} for Ag2* and Ag3*. Finally, we note the existence of a tetrahedral mode position (Cu1*), not observed in γ-Ag_7PSe_6. These observations, along with the lower atomic equivalent IDPs already mentioned, suggest a lower ionic conductivity for γ-Cu_7PSe_6, with higher mobility activation energies for Cu^+ cations and therefore more localized time-averaged probability densities. This is in agreement with a prevailing idea, *i.e.* the silver compounds are better ionic conductors than their copper homologues (McOmber *et al.*, 1980).

An analysis of the copper most probable environment based upon the Cu-mode to Se-atom distances ascertain the

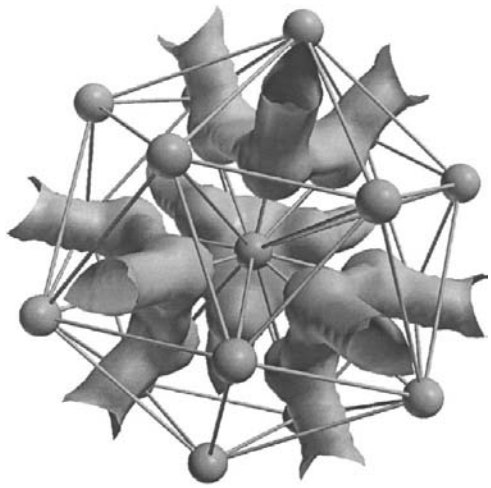

Figure 3
Three-dimensional representation of joint probability density isosurface (at the 20 Å^{-3} level) for γ-Cu_7PSe_6 at 353 K. No connection is observed between clusters around the central Se2 atom.

Table 5
Main interatomic distances (Å).

Positions with asterisks refer to the Cu1* (0.0725, −0.0819, −0.2683), Cu2*b* (0.0626, 0.0570, 0.2651) and Cu3* (0.3655, 0.3655, 0.3655) mode positions for β-Cu_7PSe_6 (for Cu2*b* the mode position corresponds to the refined position) and Cu1* (0.0700, 0.0700, 0.2669), and Cu2* (0, 0, 0.2797) mode positions for γ-Cu_7PSe_6 (for Cu3 the mode position coincides with the mean position).

β-Cu_7PSe_6 (T = 293 K)		γ-Cu_7PSe_6 (T = 353 K)	
PSe_4 sites			
P—Se1*a*	2.210 (2) (×1)	P—Se1	2.2028 (5) (×4)
P—Se1*b*	2.199 (2) (×3)		
⟨P—Se⟩	2.202	⟨P—Se⟩	2.203
$CuSe_2$ sites			
Cu3*—Se2	2.2636 (11) (×1)	Cu3—Se2	2.127 (8) (×1)
Cu3*—Se3	2.1971 (12) (×1)	Cu3—Se3	2.252 (8) (×1)
⟨Cu3*—Se⟩	2.230	⟨Cu3—Se⟩	2.190
$CuSe_3$ sites			
Cu2*a*—Se3	2.326 (3) (×1)	Cu2*—Se3	2.2279 (×1)
Cu2*a*—Se1*b*	2.382 (7) (×1)	Cu2*—Se1	2.373 (5) (×2)
Cu2*a*—Se1*b*	2.423 (7) (×1)		
⟨Cu2*a*—Se⟩	2.377	⟨Cu2*—Se⟩	2.325
$CuSe_4$ sites			
Cu1*—Se2	2.4849 (11) (×1)	Cu1*—Se1	2.4982 (5) (×2)
Cu1*—Se1*a*	2.5056 (9) (×1)	Cu1*—Se3	2.5611 (×1)
Cu1*—Se1*b*	2.5246 (10) (×1)	Cu1*—Se2	2.5800 (×1)
Cu1*—Se3	2.5667 (12) (×1)		
⟨Cu1*—Se⟩	2.520	⟨Cu1*—Se⟩	2.534
Cu2*b**—Se1b	2.4357 (11) (×1)		
Cu2*b**—Se1*b*	2.5253 (11) (×1)		
Cu2*b**—Se2	2.5310 (11) (×1)		
Cu2*b**—Se3	2.6203 (12) (×1)		
⟨Cu2*b**—Se⟩	2.528		
Shortest Cu—Cu contacts in β-Cu_7PSe_6			
Cu2*b**—Cu2*a*	0.833 (9)		
Cu1*—Cu2*b**	2.416		
Cu1*—Cu2*a*	2.855 (8)		
Cu1*—Cu2*a*	2.865 (8)		
Cu2*b**—Cu2*b**	2.928		
Cu2*b**—Cu2*a*	2.954 (8)		

structural model viability. The average Cu1*—Se distance (2.534 Å, see Table 5) is comparable to that calculated in $Cu_{1.8}Se$ for tetrahedral sites (2.496 Å; Heyding & MacLaren Murray, 1976) and close to the value given in Shannon's table (2.475 Å). Similarly, the average Cu2*—Se distance found in the triangular-like site (2.32 Å) corresponds to that found in $Cu_{1.8}Se$ for a similar coordination (2.354 Å). The last Cu*—Se average distance (d_{Cu3^*-Se} = 2.19 Å) cannot be easily compared to known distances since Cu^+ has never been found, to our knowledge, in linear selenium environments. Let us now consider β-Cu_7PSe_6, obtained after copper localization in preferential sites, and see if this particular environment is preserved.

4.2. β-Cu_7PSe_6 (293 K)

The main difficulty encountered in the structure determination of β-Cu_7PSe_6 was the twinning (see above). To analyze that twinning, several thermal treatments of RT1 and RT3 single crystals have been performed. RT1 and RT3 crystals were reanalyzed at room temperature after a high-temperature cycling through the γ-Cu_7PSe_6 form and a low-temperature cycling through the α-Cu_7PSe_6 form, respectively. The twinning fractions were found to be identical, within the standard deviation, before and after the thermal treatment [24.1 (3) and 25.3 (5)% for RT1 and 55.1 (4) and 53.3 (3)% for RT3, respectively]. The twinning seems, therefore, intrinsic to the crystals. MAS NMR studies agreed with the loss of the $\bar{4}3m$ local symmetry by the P atoms when going through the $\gamma \rightarrow \beta$ transition, which implies a splitting of the Se1 position into Se1*a* and Se1*b* (with a multiplicity ratio of 1:3). In fact, MAS NMR studies have shown that the only possible space groups were $P\bar{4}3m$, $P2_13$ and $P23$, $P2_13$ being the only one compatible with the X-ray data.

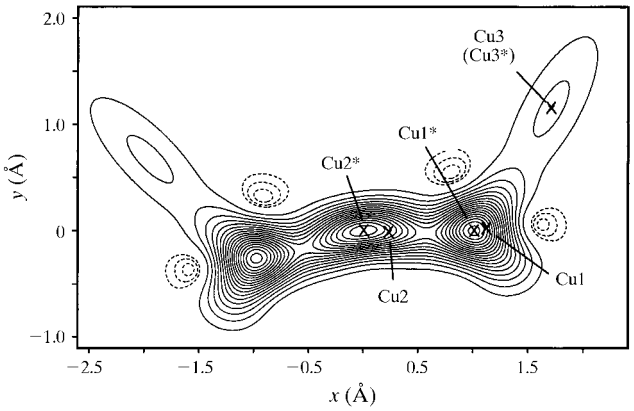

Figure 4
Non-harmonic joint probability density function map of copper for γ-Cu_7PSe_6 (353 K); section defined by the Cu1*, Cu2* and Cu3* mode positions (indicated by ×); contour lines for −30, −20 and −10 $Å^{-3}$ (dashed lines) and from 100 to 2200 $Å^{-3}$ in intervals of 100 $Å^{-3}$ (continuous lines).

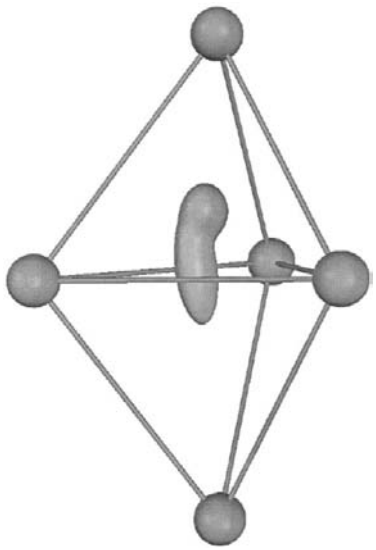

Figure 5
Three-dimensional representation of a joint probability density isosurface (at the 500 $Å^{-3}$ level) for Cu2*a* and Cu2*b* in β-Cu_7PSe_6 (293 K). Se atoms are represented as spheres of arbitrary size.

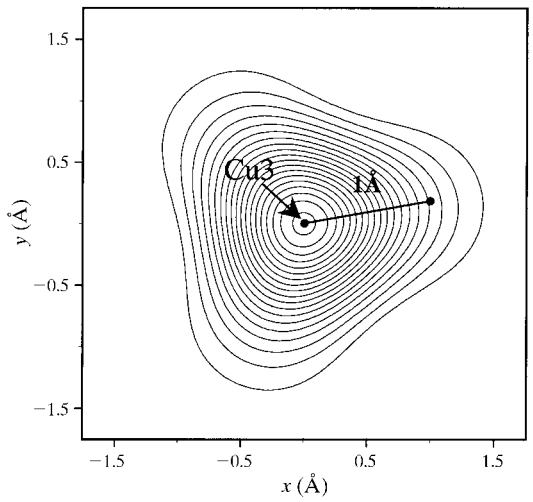

Figure 6
Non-harmonic joint probability density function map of copper Cu3 for β-Cu_7PSe_6 (293 K); section perpendicular to the [111] direction and crossing the Cu3 position; contour lines from 100 to 1900 Å^{-3} in intervals of 100 Å^{-3}.

As expected, in β-Cu_7PSe_6 an ordering of copper occurs and the Cu^+ cations occupy positions close to the modes observed in γ-Cu_7PSe_6. Cu1 is found in a tetrahedral site with a mode position calculated close to the refined mean position and with the usual Cu—Se distances for such a site (d_{Cu1^*-Se} = 2.52 Å in average). Cu2 is distributed over two close positions, a tetrahedral site similar to that of Cu1 (d_{Cu2b^*-Se} = 2.53 Å on average) and a triangular-like site (d_{Cu2a^*-Se} = 2.38 Å on average). The two Cu2*a* and Cu2*b* probability density functions strongly overlap, as shown in Fig. 5, denoting a possible movement of copper between the two positions. In a similar way, the Cu3 probability density function is spread over a large area around the threefold axis (see Fig. 6), giving rise to a very large equivalent IDP (U_{eq} = 0.2 Å^2). This was not the case in β-Ag_7PSe_6, where Ag2 was mainly found in the triangular site (only slightly displaced toward the tetrahedral center) and where Ag3 had a much lower equivalent IDP (U_{eq} = 0.07 Å^2). Those observations suggest that Cu is not stable in selenium linear environments, which could be at the origin of the last $\beta \rightarrow \alpha$ transformation at lower temperature. The ADPs observed for the skeleton atoms, P and Se, are lower than those found in γ-Cu_7PSe_6, in conformity with the localized character of the structure.

5. Conclusions

The structure determination of two of the three polymorphic forms of Cu_7PSe_6, in comparison to that realised for Ag_7PSe_6, reveals the essential differences between Cu and Ag d^{10} cations. First, it shows that, as expected, copper is less mobile than silver, the diffusion path being less pronounced and the probability density function more localized for copper than for silver. Second, it suggests that copper is less stable in selenium low coordination (in particular linear coordination) than silver, a usual observation in chalcogenides. The structure determination of α-Cu_7PSe_6 should bring new insights on the effective stability of Cu^+ in linear selenium environments.

References

Andrae, H. & Blachnik, R. (1993). *J. Thermal Anal.* **39**, 1031–1038.
Becker, P. J. & Coppens, P. (1974). *Acta Cryst.* A**30**, 129–147.
Boucher, F., Evain, M. & Brec, R. (1993). *J. Solid State Chem.* **107**, 332–346.
Creagh, D. C. & McAuley, W. J. (1992). *International Tables for X-ray Crystallography*, edited by A. J. C. Wilson, Vol. C, ch. 4.2. Dordrecht: Kluwer Academic Publishers.
Evain, M., Gaudin, E., Boucher, F., Petricek, V. & Taulelle, F. (1998). *Acta Cryst.* B**54**, 376–383.
Heyding, R. & MacLaren Murray, R. (1976). *Can. J. Chem.* **54**, 841–848.
Johnson, C. K. & Levy, H. A. (1974). *International Tables for X-ray Crystallography*, edited by J. A. Ibers and W. C. Hamilton, Vol. IV, pp. 311–336. Birmingham: Kynoch Press.
Kuhs, W. F. (1983). *Acta Cryst.* A**39**, 148–158.
Kuhs, W. F. (1984). *Acta Cryst.* A**40**, 133–137.
Kuhs, W. F., Schulte-Kellinhaus, M., Krämer, V. & Nitsche, R. (1977). *Z. Naturforsch. Teil B*, **32**, 1100–1101.
Maslen, E. N., Fox, A. G. & O'Keefe, M. A. (1992). *International Tables for X-ray Crystallography*, edited by A. J. C. Wilson, Vol. C, ch. 6.1. Dordrecht: Kluwer Academic Publishers.
McOmber, J. I., Topiol, S., Ratner, M. A. & Shriver, D. F. (1980). *J. Phys. Chem. Solids*, **41**, 447–453.
Petricek, V. & Dusek, M. (1998). *JANA98.* Institute of Physics, Academy of Sciences of the Czech Republic, Prague, Czech Republic.
Shannon, R. D. (1981). *Structure and Bonding in Crystals*, edited by M. O'Keeffe and A. Navrotsky, Vol. II, pp. 53–70. Academic Press.